SQU Journal for Science, 2020, 25(2), 112-123 DOI:10.24200/squjs.vol25iss2pp112-123
Sultan Qaboos University

Effects of Thermal Stratification and Anisotropic Porous Material in a Symmetrically Heated Vertical Channel

Basant K. Jha, Muhammad K. Musa* and Abiodun O. Ajibade

Department of Mathematics, Ahmadu Bello University, Zaria, Nigeria, *Email*: mmkabirxy@yahoo.com.

ABSTRACT: The coexistence in nature of thermally stratified fluids and directionally inclined porous structures abound in geophysical fluid flow. Despite their important applications especially in underground flow, their combined effects on natural convection have not been intensively investigated. This article aims to investigate a fully developed time dependent natural convection of viscous incompressible stably stratified fluid in the presence of anisotropic porous material. The semi analytical solutions of the governing equations for the temperature and velocity fields are obtained using the Laplace Transform Technique, Riemann Sum Approximation and D'Alembert Methods. The choice of the D'Alembert Method is to provide a systematic decoupling procedure for the coupled governing equations while still retaining their original orders. This research establishes that the fluid maximum or minimum velocity can be attained by properly manipulating the anisotropic parameters.

Keywords: Transient free convection; Anisotropic porous materials; Stably stratified fluid; Riemann Sum Approximation; D'Alembert Method; Symmetric heating.

تأثيرات الطبقات الحرارية والمواد المسامية متباينة الخواص على قناة عمودية تُسخَّنْ بالتساوي

بسنت ك. جاه، ومحمد ك. موسى وأبيدون و. أجيباد

الملخص: إن التعايش في طبيعة السوائل الطبقية حرارياً والهياكل المسامية تميل إلى تدفق السوائل الجيوفيزيائية. على الرغم من تطبيقاتها المهمة خاصة في التدفق الجوفي، فإنه لم يتم دراسة آثارها المشتركة بشكل مكثف على الحمل الحراري الطبيعي. يهدف هذا البحث إلى دراسة الحمل الحراري الطبيعي المطوّر بالكامل والمعتمد على زمن السائل اللزج غير القابل للضغط الطبقي المستقر بوجود مادة مسامية متباينة الخواص. يتم الحصول على الحلول شبه التحليلية لمعادلات التحكم في مجالي الحرارة والسرعة باستخدام تحويلات لابلاس وتقريب مجموع ريمان وطريقة د،المبرت. إن اختيار طريقة د،المبرت يؤدي إلى فصل منظم لمعادلات التحكم المقترنة مع الاحتفاظ بدرجاتها الأصلية. أثبتت الدراسة أنه يمكن تحقيق السرعة القصوى أو الدنيا للسائل من خلال تغيير مقبول للمؤثرات متباينة الخواص.

الكلمات المفتاحية: الحمل الحراري العابر؛ مواد مسامية متباينة الخواص؛ سائل طبقي مستقر؛ تقريب مجموع ريمان؛ طريقة د،المبرت؛ التسخين بالتساوي.

1. Introduction

Analytical and numerical study of free convective fluid flow through porous materials continues to receive considerable attention in the literature. This is as a result of their wide industrial and technological applications such as in noise reduction in aerodynamics [1], combustion devices [2], biological systems and biotechnology [3], waste water treatment plants [4] and in nuclear reactors [5]. As a result of these endless important applications, investigations involving the impact of a porous matrix in fluid flow formation is still on-going. Thus, by taking the Hall effect into account, [6] have examined the peristaltic transport of Williamson fluid through a porous medium. The results of the investigation on peristaltic flow of a compressible Maxwell fluid resulting from the surface acoustic wave in a parallel-plane micro-channel through a porous medium in the presence of a constant magnetic field have been presented by [7]. [8] Investigated the peristaltic motion in a gall bladder induced by the sinusoidal traveling wave and noted that the Hall parameter enhances the mean velocity distribution, the reversal flow and the perturbation function.

According to Khaled and Vafai [9], in an attempt to investigate the role of porous media in the transport processes, the classical (Darcy) model, which simply presents a linear relationship between the superficial average velocity (U) and the pressure difference (P) applied across the porous medium, was developed. As a result of its limitations, the Darcy Model was later extended to account for cases where large fluid flow (Forchheirmen's Model) and boundary effects (Brinkman's Model) are required.

It is important to state here that most of the earlier investigations of natural convection through porous media (such as Vafai [10] and Pop and Ingham [11]) were conducted on the basis of the following assumptions: (a) that the ambient flow media outside the flow regions were taken to be of uniform density as well as at constant temperature (isothermal) and (b) the preferential direction of some physical quantities such as the permeability of the beads or fibers of the porous media were generally neglected (isotropic). These assumptions failed to capture the true forms in which geophysical fluids, especially, are encountered in nature, as well as how naturally existing or artificially developed porous media behave.

Several types of research where the fluid density in the ambient medium is non-uniform and varies with height are currently being investigated. This phenomenon, which has an over bearing effect on natural convection due to density variation, is termed in the existing literature as 'stratification of the media'. Several applications ranging from cooling circuit boards in electronic devices to the triggering of heat circulation in the atmosphere which influences weather conditions abound in industry and in nature. Stratification generally consists of fluid layers of different densities such that, under gravitational influence, they are arranged so that fluids of higher densities are found beneath those of lower densities.

Publications on the role played by thermal stratification on the heat convection processes include the demonstration of the effect of thermally stratified ambient fluid on MHD by Gurminder *et al.* [12]. Deka and Paul [13, 14] have shown that thermal stratification suppresses the fluid momentum in the boundary layer and also observe that stratification transforms the transient state to a steady state as time progresses. Shapiro and Fedorovich [15] presented an analytical description of the steady shallow convective flow of a viscous and diffusive stably stratified fluid over a differentially heated lower boundary. In a controlled laboratory experiment, Falasca *et al.* [16] took a stratified atmospheric boundary layer into account, and analyzed the simulations of an urban heat island. Another excellent research work worth mentioning here is the impact of stably stratified fluid in the presence of Magneto-hydrodynamic (MHD) conducted by Deka and Bhattacharya [17].

In studying transport problems, especially when a porous medium is incorporated into the transport equation, consideration of the orientation of the fibers or beads of the porous matrix becomes very interesting. Anisotropy results from the preferential orientation of the grains or fibers that constitute the porous structure. Thus, while investigating heat transfer in the presence of anisotropic porous medium with oblique principal axes, Vajravelu and Prasad [18] observed that anisotropy is characterized by the ratio of permeability $\left(k^* = \frac{k_1}{k_2}\right)$ and the angle of orientation (φ) between the horizontal direction and principal axis k_2 with the permeability. Bera and Khalili [19] suggest that the permeability of the porous media act as a conductivity of the fluid flow and that for large values of anisotropic permeability ratio, $(k^* > 1)$, a decrease in the anisotropic angle of orientation (θ), within the closed interval $[0^o, 90^o]$, enhances the total permeability along the main flow direction, which consequently aids in strengthening the fluid convection current. Expressing the penetration length of the convective flow and heat transfer rate in terms of the anisotropic properties of the porous medium, Karmakar and Sekhar [20] demonstrated that the directional permeability of the anisotropic porous structure greatly influences the fluid flow through a composite porous channel. In another investigation, Yovogan and Degan [21] established that anisotropic parameters can be used to predict environmental aquatic behaviour. Other reports on the various roles played by anisotropy parameters can also be found in Degan *et al.* [22], Filip *et al.* [23], and Filip *et al.* [24].

In all the above cases examined, the influence of anisotropy and thermal stratification on temperature and fluid velocity are studied separately. The purpose of the present article is to simultaneously examine the combined effects of thermal stratification and anisotropic porous material on the transient free convective mode of fluid flow in a symmetrically heated vertical channel. The semi-analytical solution presented in this article expands the data base of known analytical/semi-analytical solutions for transient natural convection flow in a channel filled with anisotropic porous material in a stably stratified medium.

2. Mathematical Analysis

Consider the problem of time dependent natural convection in a symmetrically heated vertical channel as depicted in figure 1.0. The coordinate systems of the problem are selected in such a way that the $y - axis$ is the direction of the fluid flow and perpendicular to the gravitational pull and the channel walls while the $x - axis$ is parallel to them. The fluid occupying the region $-h \leq y' \leq h$ is assumed to be thermally stratified. According to Deka and Paul [13], thermal stratification is as a result of the combined effects of $\frac{dT_\infty(x')}{dx'}$; the ambient fluid temperature (or vertical advection) which depends on the height x' of the transport medium, and $\frac{g}{C_p}$, the rate of reversible work done on the fluid particles by compression. Here, $T_\infty(x')$ is the varying environmental temperature, g is the gravitational constant and C_p is the specific heat capacity of the fluid at a constant pressure. In the present investigation, the working

fluid is air ($Pr = 0.71$) so that $C_p = 1012JKg^{-1}K^{-1}$. As a result, the work of compression on the air particle $\frac{g}{C_p}$ is negligible since $g = 9.8\,ms^{-2}$. Hence the thermal stratification can therefore be seen as being dominated by the vertical advection temperature term. Accordingly, three possible situations exist: (i) the adiabatic or neutral ($S' = 0$) case which, according to Deka and Paul [14], represents the largest rate at which temperature can decrease with height without resulting in instability (ii) unstable stratification ($S' < 0$), in which less dense fluid exists at the bottom of a denser fluid and (iii) stable stratification ($S' > 0$), which characterizes the scenario where the less dense fluid is found at the top of the denser fluid. This last characterization is the focus of this research.

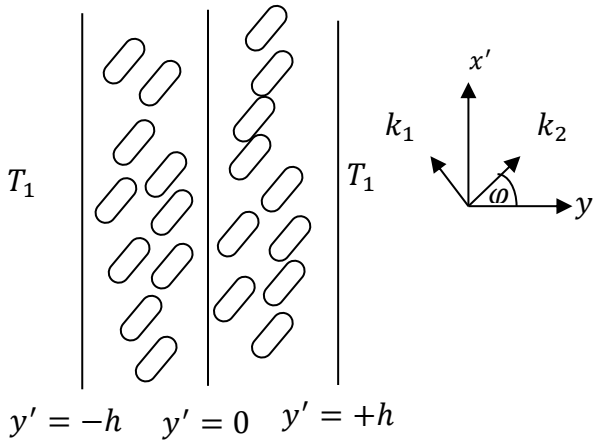

Figure 1. Schematic diagram of the problem.

Further, it is assumed that the channel is saturated with anisotropic porous materials. Anisotropic porous structure is characterized by the ratio of permeability of the porous material; $k^* = \frac{k_1}{k_2}$ and the angle of orientation φ which is the angle between the horizontal direction and principal axis k_2 with the permeability. At $t' \leq 0$, both the stratified fluid and the channel walls are maintained at a temperature T_0. At time $t' > 0$, the natural convective process is triggered by the symmetric heating of the bounding walls from the initial thermodynamically equilibrium ($T' = T_0$) state to $T' = T_1$. Under these assumptions, and following Degan *et al*. [22] and Deka and Bhattacharya [17] the governing equations for fluid velocity and temperature distributions are given as follows:

$$\frac{\partial U'}{\partial t'} = \upsilon_{eff}\frac{\partial^2 U'}{\partial y'^2} - \frac{U'\upsilon}{\bar{\bar{K}}} + g\beta(T' - T_0) \tag{1}$$

$$\frac{\partial T'}{\partial t'} = \frac{k}{\rho C_p}\frac{\partial^2 T'}{\partial y'^2} - S'U' \tag{2}$$

Due to the symmetric heating of the channel walls, the initial and boundary conditions consistent with the physical situation are:

$$t' \leq 0, \quad T' = T_0, \quad U' = 0 \quad at \quad -\mathrm{h} \leq y' \leq +h$$

$$\begin{cases} t' > 0 \ \frac{\partial U'}{\partial y'} = 0, \ \frac{\partial T'}{\partial y'} = 0 & \text{at} \quad y' = 0 \\ U' = 0, \ T' = T_1 & at \quad y' = +h \end{cases} \tag{3}$$

where the second order symmetric tensor $\bar{\bar{K}}$ is defined as:

$$\bar{\bar{K}} = \begin{bmatrix} k_1 cos^2(\varphi) + k_2 sin^2(\varphi) & (k_1 - k_2)sin(\varphi)cos(\varphi) \\ (k_1 - k_2)sin(\varphi)cos(\varphi) & k_2 cos^2(\varphi) + k_1 sin^2(\varphi) \end{bmatrix} . \tag{4}$$

Introducing the following non-dimensional quantities

$U = \frac{U'\mathrm{h}}{\upsilon}$, $T = \frac{T' - T_0}{T_1 - T_0}$, $y = \frac{y'}{h}$, $\gamma = \frac{\upsilon_{eff}}{\upsilon}$, $t = \frac{t'\upsilon}{\mathrm{h}^2}$, $S = \frac{S'h}{T_1 - T_0}$, $\mathrm{Pr} = \frac{\upsilon\rho C_p}{k}$, $Da = \frac{k_1}{h^2}$ and $Gr = \frac{g\beta(T_1 - T_0)\mathrm{h}^3}{\upsilon^2}$

equations (1)-(3) can then be expressed in dimensionless form as:

$$\frac{\partial U}{\partial t} = \gamma\frac{\partial^2 U}{\partial y^2} - a\frac{U}{Da} + GrT \tag{5}$$

$$\frac{\partial T}{\partial t} = \frac{1}{Pr}\frac{\partial^2 T}{\partial y^2} - SU \tag{6}$$

where $a = cos^2(\varphi) + k^* sin^2(\varphi)$ is obtained from equation (4) and the initial and boundary conditions now assume the following form:

$$\begin{cases} t \le 0;\ U = 0,\ T = 0 & \text{at} \quad 0 \le y \le 1 \\ t > 0;\ \frac{\partial U}{\partial y} = 0,\ \frac{\partial T}{\partial y} = 0 & \text{at} \quad y = 0 \\ U = 0, \quad T = 1 & \text{at} \quad y = 1 \end{cases} \tag{7}$$

2.1 Solutions

Since equations (5) and (6) are second order coupled Partial Differential Equations, Laplace Transform Techniques defined for any arbitrary function as $\bar{f}(y,t) = \int_0^\infty Fe^{-pt}dt$, are employed to produce coupled second order Ordinary Differential Equations:

$$\frac{d^2\bar{U}}{dy^2} - \frac{\bar{U}}{\gamma}\left(p + \frac{a}{Da}\right) = -\frac{\mathrm{Gr}}{\gamma}\bar{T} \tag{8}$$

$$\frac{d^2\bar{T}}{dy^2} - SPr\bar{U} - pPr\bar{T} = 0 \tag{9}$$

Where in order to ensure convergence, the Laplace parameter $p > 0$. It is observed that equations (8) and (9) are coupled second order Ordinary Differential Equations in the Laplace domain. Attempting to solve these equations by directly eliminating the velocity (or temperature) will simply lead to solving a set of complex couple equations of a higher order. Thus, in this research, the D'Alembert method (Ziyaddin and Huseyin [25]) is used. This method allows for the systematic decoupling of the governing equations while still retaining their initial orders.

Multiplying through equation (8) by D and adding the resulting equation to equation (9) produces:

$$\frac{d^2}{dy^2}(D\bar{U} + \bar{T}) - \delta^2(D\bar{U} + \bar{T}) = 0 \tag{10}$$

Where the quadratic function in terms of D is chosen and defined as:

$$D^2 + \frac{D}{Gr}\left(P + \frac{a}{Da} - \gamma pPr\right) + \frac{\gamma SPr}{Gr} = 0 \quad . \tag{11}$$

Similarly

$$\delta^2 = \frac{\gamma pPr - DGr}{\gamma} \quad . \tag{12}$$

The general solution of equation (10) is obtained and is given as:

$$D\bar{U} + \bar{T} = A_1\cosh(\delta y) + A_2\sinh(\delta y) \tag{13}$$

By applying the boundary conditions (7) on equation (13), the expressions for A_1 and A_2 are obtained (see Appendix B) so that the equation (13) becomes:

$$D\bar{U} + \bar{T} = \frac{1}{p}\left(\frac{\cosh(\delta y)}{\cosh(\delta)}\right) \tag{14}$$

Replacing D and δ in equations (14) with their corresponding roots: D_1, D_2, and δ_1, δ_2 respectively (see Appendix B) obtained by solving equations (11) and (12) one after the other, yields**:**

$$D_1\bar{U} + \bar{T} = \frac{1}{p}\left(\frac{\cosh(\delta_1 y)}{\cosh(\delta_1)}\right) \tag{15}$$

$$D_2\bar{U} + \bar{T} = \frac{1}{p}\left(\frac{\cosh(\delta_2 y)}{\cosh(\delta_2)}\right) \tag{16}$$

Solving these equations simultaneously, the expressions for the velocity and temperature profiles in the Laplace domain are obtained and presented as:

$$\bar{U} = \frac{1}{p(D_1 - D_2)}\left[\frac{\cosh(\delta_1 y)}{\cosh(\delta_1)} - \frac{\cosh(\delta_2 y)}{\cosh(\delta_2)}\right] \tag{17}$$

$$\bar{T} = \frac{1}{p(D_1 - D_2)}\left[\frac{D_1\cosh(\delta_2 y)}{\cosh(\delta_2)} - \frac{D_2\cosh(\delta_1 y)}{\cosh(\delta_1)}\right] \tag{18}$$

3. Nusselt number, skin friction, and volumetric mass flow rate

In order to understand the behaviour of the heat being transferred from the wall surface into the channel, the frictional force developed at the wall-fluid interface, which tends to hinder the fluid flow and the amount of fluid flowing per unit area, the rate of heat transfer $\left(\bar{N}u_1 = \frac{d\bar{T}(y,p)}{dy}\Big|_{y=1}\right)$, skin friction$\left(\bar{\tau}_1 = \frac{d\bar{U}(y,p)}{dy}\Big|_{y=1}\right)$, and volumetric mass flow $\left(\bar{Q} = \int_0^1 \bar{U}(y,p)dy\right)$ are respectively investigated. The expressions for these physical quantities are derived and presented as follows:

$$\bar{N}u_1 = \frac{1}{p(D_1 - D_2)}\left[\frac{D_1\delta_2\sinh(\delta_2)}{\cosh(\delta_2)} - \frac{D_2\delta_1\sinh(\delta_1)}{\cosh(\delta_1)}\right] \tag{19}$$

$$\bar{\tau}_1 = \frac{1}{p(D_1 - D_2)}\left[\frac{\delta_1\sinh(\delta_1)}{\cosh(\delta_1)} - \frac{\delta_2\sinh(\delta_2)}{\cosh(\delta_2)}\right] \tag{20}$$

$$\bar{Q} = \frac{1}{p(D_1 - D_2)}\left[\frac{\sinh(\delta_1)}{\delta_1\cosh(\delta_1)} - \frac{\sinh(\delta_2)}{\delta_2\cosh(\delta_2)}\right] \tag{21}$$

To convert equations (17)-(21) to their corresponding time domain, their respective Laplace inverses are obtained. This, however, would be complicated to achieve, hence a numerical approach based on the Riemann-Sum approximation method is employed. According to Jha and Apere [26] and Jha and Isa [27] the Laplace inverse of any function $\bar{U}(y,p)$ can be approximated by:

$$U(y,t) = \frac{e^{\varepsilon t}}{t}\left[\frac{1}{2}\bar{U}(y,\varepsilon) + Re\sum_{k=1}^{n}\bar{U}\left(y,\varepsilon + \frac{ik\pi}{t}\right)(-1)^k\right] . \tag{22}$$

In this representation, Re and $i = \sqrt{-1}$ are real and imaginary numbers respectively, and n is the number of iterations used in the method. If the number of iterations must be minimized and faster convergence is to be achieved, it was suggested (Tzou [28]) that the product of the time (t) and the real part of Bromwich contour (ε) used for inverting a function from the Laplace domain to its corresponding time domain should be 4.7.

By appropriately replacing $\bar{U}(y,p)$, the Laplace inverses of equations (18)-(21) can similarly be obtained.

4. Validation of the Semi-Analytical Method used: Steady State Model

In order to establish the accuracy of the semi-analytical approach employed in computing the transient state solutions, the corresponding steady state solutions for the velocity and temperature equations have been derived analytically. The transient states results obtained are compared with the results from steady states (see Paul *et al*. [29]). Thus, by setting $\frac{\partial U}{\partial t} = 0$ and $\frac{\partial T}{\partial t} = 0$ in equations (5) and (6) respectively, the steady state mathematical model is obtained:

$$\frac{d^2U}{dy^2} - a\frac{U}{\gamma Da} = -\frac{TGr}{\gamma} \tag{23}$$

$$\frac{d^2T}{dy^2} - prSU = 0 \tag{24}$$

and the corresponding boundary conditions become:

$$\left.\begin{array}{llll} \frac{dU}{dy} = \frac{dT}{dy} = 0, & \text{at} & y = 0 \\ U = 0, \quad T = 1 & \text{at} & y = 1 \end{array}\right\} \tag{25}$$

The exact solutions of equations (23) and (24) satisfying the boundary conditions (25) are obtained by using the D'Alembert method and are given as:

$$U = \frac{1}{(B_1 - B_2)}\left[\frac{\cosh(\alpha_2 y)}{\cosh(\alpha_2)} - \frac{\cosh(\alpha_1 y)}{\cosh(\alpha_1)}\right] \tag{26}$$

$$T = \frac{1}{(B_1 - B_2)}\left[\frac{B_1\cosh(\alpha_2 y)}{\cosh(\alpha_2)} - \frac{B_2\cosh(\alpha_1 y)}{\cosh(\alpha_1)}\right] \tag{27}$$

The expressions for B_1, B_2, α_1 and α_2 are presented in Appendix B

Table 1. Comparison between transient state (Riemann-Sum Approximation Method) and steady state (exact solution) velocity and temperature distributions.

t	*y*	Transient	
		Velocity	Temperature
0.5	0.2	0.5484	0.7367
	0.4	0.5230	0.5091
	0.6	0.3619	0.3180
	0.8	0.1801	0.1526
1.0	0.2	0.5485	0.7368
	0.4	0.5231	0.5092
	0.6	0.3621	0.3182
	0.8	0.1802	0.1527

t	*y*	Transient	
		Velocity	Temperature
1.5	0.2	0.5484	0.7367
	0.4	0.5231	0.5092
	0.6	0.3621	0.3182
	0.8	0.1802	0.1527
Steady State	0.2	0.5485	0.7367
	0.4	0.5231	0.5092
	0.6	0.3621	0.3182
	0.8	0.1802	0.1527

It is observed from table 1.0 that the numerical results for the transient state velocity and temperature distributions obtained with the Riemann Sum Approximation Method agree excellently with the numerical values for the exact solutions for the steady state velocity and temperature as $t \to Pr$. Thus, this result further confirms the accuracy of the Riemann Sum Approximation method employed.

5. Results and Discussion

In order to have an insight into the present problem, numerical computations for velocity, temperature, skin friction, rate of heat transfer and volumetric mass flow rate are performed for different values of the controlling parameters. Line graphs and contour maps (figures. 2-19) are depicted for transient state temperature and velocity profiles along with those of Nusselt number, skin friction, and volumetric mass flow rate to clearly show the influence of these parameters.

First, the accuracy of the results obtained needs to be confirmed. To achieve this, tables 2.0 and 3.0 have been constructed. It is clear that for $Pr = 0.71$ (air) and $Pr = 7.0$ (water), by neglecting the anisotropic parameter as well as allowing the vertical advection to coincide with the rate of reversible work done on the fluid particles by compression, the numerical data generated for the present research favourably compare with the numerical results provided by Jha [30] with respect to skin friction, and by Jha and Singh [31] with respect to skin friction and volumetric mass flow rate, as seen in table 2.0 and table 3.0 respectively.

Table 2. Comparing the numerical values of Skin friction (τ) for water $(Pr = 7.0)$ in the work of Jha [30] and the present work in the absence of anisotropic and thermal stratification parameters.

	Jha [30]			Present work		
t/Da	0.5000	0.2500	0.1667	0.5000	0.2500	0.1667
0.2	0.13371	0.12945	0.12546	0.1338	0.1295	0.1259
0.4	0.18466	0.17383	0.16503	0.1847	0.1739	0.1656
0.6	0.22307	0.20454	0.19071	0.2231	0.2046	0.1915
2.0	0.38786	0.32025	0.28029	0.3880	0.3204	0.2804
4.0	0.50951	0.40216	0.34203	0.5097	0.4023	0.3422
6.0	0.56955	0.44255	0.37248	0.5697	0.4427	0.3727

Table 3. Comparing Skin friction (τ) and Mass flow rate (Q): - Jha and Singh [31] and the present work in the absence of anisotropic and thermal stratification parameters

		Present work		Jha and Singh [31]	
Pr	t	τ	Q	τ	Q
0.71	0.4	0.4526	0.1115	0.4523	0.1114
	0.6	0.6108	0.1756	0.6105	0.1754
	1.0	0.8246	0.2622	0.8242	0.2620
7.0	0.4	0.1984	0.0195	0.1983	0.0195
	0.6	0.2496	0.0349	--------	0.0348
	1.0	0.3424	0.0684	0.3422	0.0683

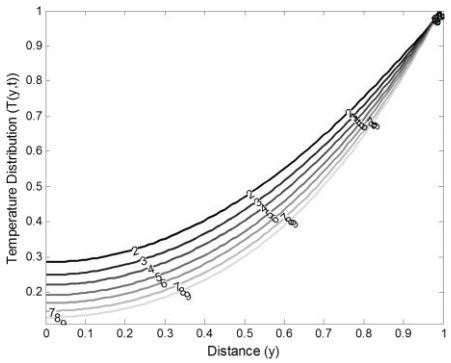

Figure 2. Temperature distribution for different S with $Pr = 0.71$, $\varphi = 45^0$, $t = 0.4, Da = 0.01$, Gr=70.0, $\gamma = 1.5$ and $k^* = 0.2$

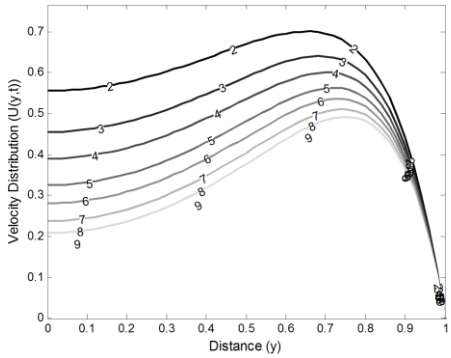

Figure 3. Velocity distribution for different S with $Pr = 0.71$, $\varphi = 45^0$, $Da = 0{,}01$, $t = 0.4$, Gr=70.0, $\gamma = 1.5$ and $k^* = 0.2$

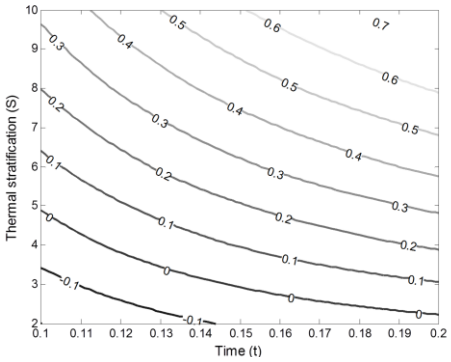

Figure 4. Rate of heat transfer for different S with $Pr = 0.71$, $k^* = 0.2$, $\varphi = 45^0$, Gr=70.0, $Da = 0.01$ and $\gamma = 1.5$

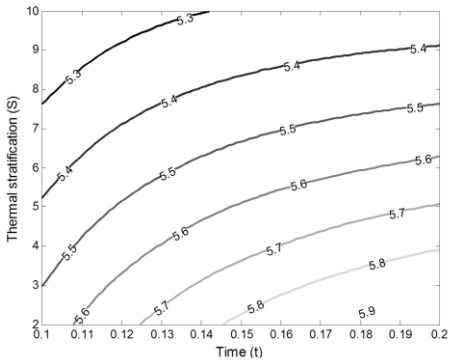

Figure 5. Skin friction for different S with $Pr = 0.71$, $k^* = 0.2$, $\varphi = 45^0$, Gr=70.0, $Da = 0.01$ and $\gamma = 1.5$

Figures 2-5 exhibit the effect of thermal stratification (S) on temperature, fluid velocity, rate of heat transfer and skin friction. As seen in the figures, an increase in the stratification parameter suppresses the temperature within the vertical channel (Figure 2) and as a result, a weak velocity current is created (Figure 3). This is because stratification creates fluid layers which increase with height. These layers create resistance (layering effects) to temperature penetration hence a decrease in both the temperature and velocity distributions are observed. The numerical simulation conducted also revealed that increasing the stratification parameter enhances the rate of heat transfer (Figure 4) but decreases the frictional force at the surface-fluid interface (Figure 5).

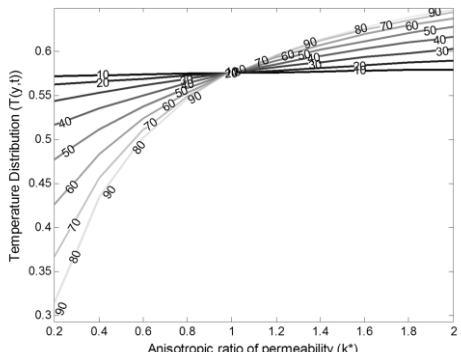

Figure 6. Temperature distribution for different φ and k^* with $Pr = 0.71, t = 0.4$, $S = 2.5, Da = 0.01$, Gr=70.0, $\gamma = 1.5$ and $\nu = 0.4$

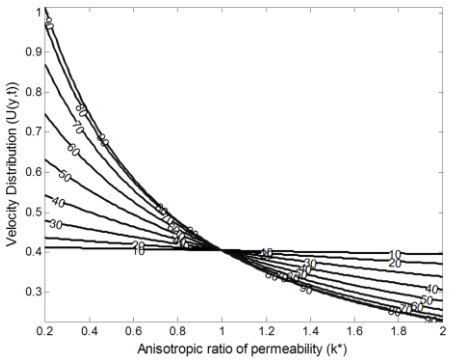

Figure 7. Velocity distribution for different φ and k^* with $Pr = 0.71, t = 0.4, S = 2.5, Da = 0.01$, Gr=70.0,

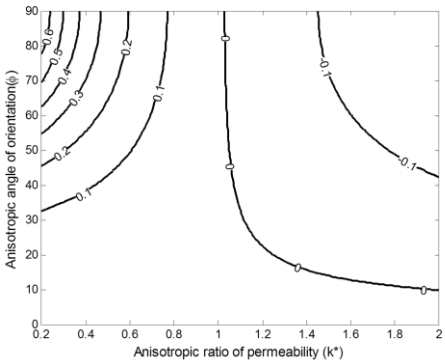

Figure 8. Rate of heat transfer for different φ and k^* with $Pr = 0.71$, $t = 0.4$, $S = 2.5$, Gr =70.0, $Da = 0.01$ and $\gamma = 1.5$

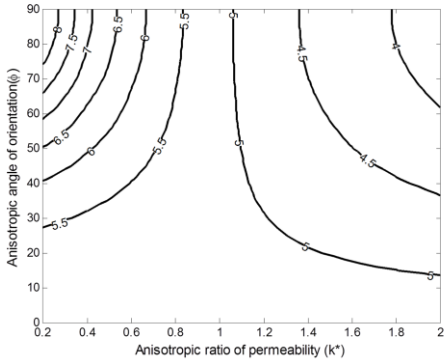

Figure 9. Skin friction for different values of φ and k^* with $Pr = 0.71$, $t = 0.4$, $S = 2.5$, Gr =70.0, $Da = 0.01$ and $\gamma = 1.5$

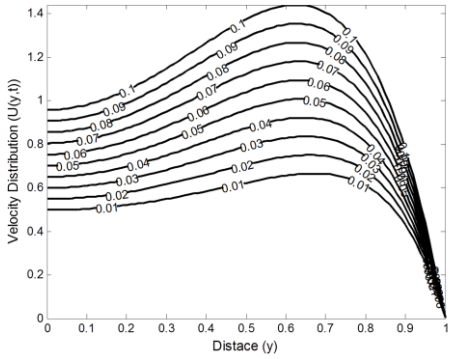

Figure 10. Velocity distribution for different Da with $Pr = 0.71$, $\varphi = 45^0$, $S = 2.5$, $t = 0.4$, Gr =70.0, $\gamma = 1.5$ and $k^* = 0.2$

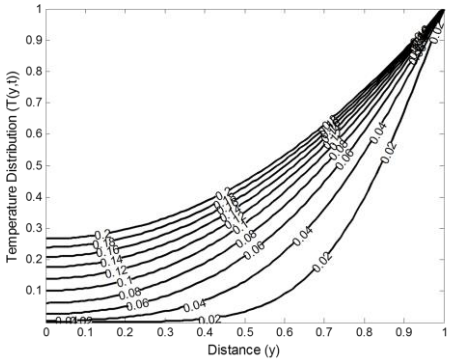

Figure 11. Temperature distribution for different t with $Pr = 0.71$, $\varphi = 45^0$, $S = 2.5$, $Da = 0.01$, Gr =70.0, $\gamma = 1.5$ and $k^* = 0.2$

The second order permeability tensor defined in equation (4) physically characterizes the direction along which fluid in an anisotropic porous system flows under imposed transport constraints. Thus from figure 1 and the expression $a = cos^2(\varphi) + k^* sin^2(\varphi)$ obtained from equation (4), if $\varphi = 90^0$ the preferential orientation of the bead or fibers of the anisotropic porous matrix becomes entirely a function of the anisotropic ratio of permeability (as $a = k^*$). In addition, it is also seen that if the angle of orientation $\varphi = 0^0$, the principal permeability axis k_2 coincides with the horizontal transverse distance (y) so that $a = 1$. This situation is identical to the case when $k^* = 1$; ($k_1 = k_2$) , as seen in Figures 6 and 7, which represents the state where the porous medium transforms to purely isotropic so that the preferential orientation of the grains of the porous structure is neglected. In particular, Figure 6 shows that if $k^* > 1$ an increase in the permeability $k_1$is observed. Consequently, an increase in temperature penetration is noticed as the anisotropic angle of orientation increases form $\varphi = 0^0$ to $\varphi = 90^0$. On the other hand, if $k^* < 1$ an increase along the permeability k_2 is observed resulting in the attenuation of fluid temperature as the angle of orientation is increased.

This behavior is transmitted into the fluid velocity distribution as depicted in figure 7. For $k^* < 1$, the fluid velocity increases as φ increases and for $k^* > 1$, the graph shows a decrease in the fluid velocity as the angle of orientation increases form $\varphi = 0^0$ to $\varphi = 90^0$. These flow trends have been observed and reported by Bera and Khalili [19]. In addition, the numerical simulation conducted indicates that both the rate of heat transfer (Figure 8) and the skin friction (figure 9) at the walls are enhanced if the anisotropic angle of orientation (φ) is increased, and for small values of the anisotropic ratio of permeability$(k^* < 1)$. If the anisotropic ratio of permeability is large $(k^* > 1)$, a converse trend is observed.

It is also interesting to note that, from the experiment conducted by Liakopoulos [32] on the permeability of soil (acting as porous material), the pores of the soil were observed to be larger when the permeability of the porous media is increased horizontally. This allows more water to flow when $k_1 < k_2$. This result explains, as seen in Figure 7, why the fluid attains its maximum velocity when $\varphi = \frac{\pi}{2}$ and minimum velocity when $\varphi = 0^0$ as $k^* < 1$. For $k^* > 1$ however, the fluid velocity is least when $\varphi = \frac{\pi}{2}$ and maximum when $\varphi = 0^0$.

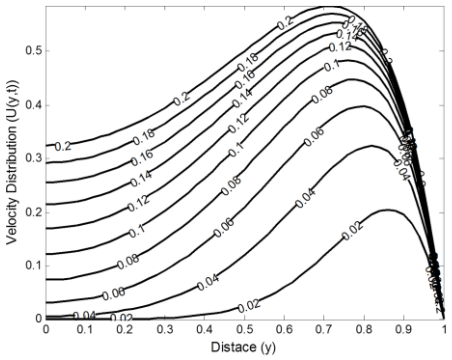

Figure 12. Velocity distribution for different t with $Pr = 0.71$, $\varphi = 45^0$, $S = 2.5, Da = 0.01$, Gr=70.0, $\gamma = 1.5$ and $k^* = 0.2$

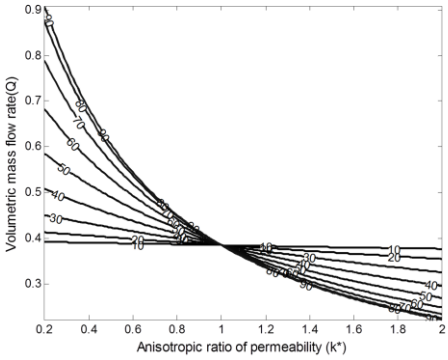

Figure 13. Mass flow rate for different values ofφ and k^* with $Pr = 0.71$, $t = 0.4$, $S = 2.5$, Gr=70.0, $Da = 0.01$ and $\gamma = 1.5$

As a result of the linear relationship that exists between the measure of permeability (Da) of the anisotropic porous medium and the principal axis k_1 with the permeability of the porous matrix, increasing the Darcy number (Da) results in an increase in the pores of the anisotropic porous medium along with permeability k_1 of the anisotropic porous structure, so that $k_1 > k_2$. This variation leads to an increase in the void of the porous passages of the anisotropic porous matrix thereby resulting in a decrease in the relative friction between the flowing fluid and porous material, and hence an increase in the fluid velocity is observed, as seen in figure 10. Figures 11 and 12 depict the influence of time (t) on both the temperature and velocity profiles. As expected, the temperature distribution in the channel saturated with an anisotropic porous matrix is observed to increase with an increase in time (t). This trend as seen in the temperature profile is replicated in the fluid velocity, as the fluid flow progresses with time.

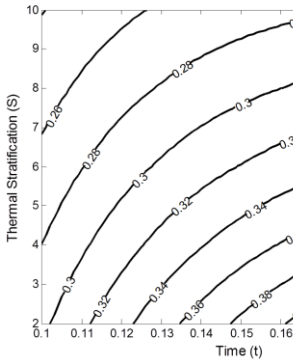

Figure 14. Mass flow rate for different values of S with $Pr = 0.71$, $\varphi = 45^0$, $k^* = 0.2$, Gr=70.0, $\gamma = 1.5$ and $Da = 0.01$

The combined roles of the anisotropic parameters (k^* and φ) and that of the thermal stratification (S) on the volumetric mass flow rate are respectively presented in Figures 13 and 14. It is observed (Figure 13) that when $k^* < 1$, increasing φ results in the increase in the volumetric mass flow rate while a converse trend is achieved when $k^* > 1$. On the other hand, the volumetric mass flow rate is observed to be suppressed with an increase in thermal stratification (S) as displayed in Figure 14.

6. Conclusion

In this paper, the Mathematical Model which takes into account the anisotropic porous material and fluid associated with vertical thermal advection and compression works on the fluid particles is investigated. Laplace transform, D'Alembert and Riemann Sum Approximation Methods are employed to obtain the solutions for the transient state governing equations. Solutions for the corresponding steady state problem were also obtained for the purpose of method validation. It was found that at $t \gg Pr$, numerical values for the transient and steady states velocity and temperature distributions coincide. Moreover, the validity of the results obtained have been established. In investigating the influence of some of the controlling parameters present in the solutions obtained, special interest is placed on the role played by anisotropy and stratification parameters. The study has established that:

i. the inclusion of the thermal stratification and anisotropic factors in the temperature and velocity equations have an overbearing influence on the physical quantities studied.

ii. in addition, due to the layering effect induced by the thermal stratification, thermal and hydrodynamic distributions in a channel have be found to be suppressed with an increase in stratification.
iii. the conditions for the attainment of maximum (or minimum) velocity with respect to the variation of anisotropic parameters have been demonstrated.

7. Future investigation and recommendations:

Researchers have constructed, and worked on another form of porous media, the bidisperse porous media. The model suggested for the porous media is for isotropy and the fluid is non-stratified. It will be interesting if anisotropy and stratification terms are included into the extended Brinkman Model for bidisperse porous media. Since the resulting model is a set of coupled equations coupling the fluid in frictional and porous phases of the porous media, the methods used in the present investigation could be very helpful.

Conflict of interest

The authors declare no conflict of interest.

Appendix A

Nomenclature

Symbol	Definitions	Units
β	coefficient of thermal expansion	$[K^{-1}]$
υ_{eff}	effective viscosity of the saturated porous media	$[m^2 s^{-1}]$
υ	kinematic viscosity of the fluid	$[m^2 s^{-1}]$
g	acceleration due to gravity	$[ms^{-2}]$
k	thermal conductivity of the fluid	$[wm^{-1}k^{-1}]$
γ	ratio of viscosities	-
C_p	specific heat of the fluid at constant pressure	$[Jkg^{-1}k^{-1}]$
k_1 and k_2	permeabilities along the principal axes of the anisotropic porous medium	$[m^2]$
k^*	ratio of anisotropy Permeability	-
φ	anisotropic angle of inclination	[Deg or Rad]
S	dimensionless stratification parameter	-
S'	dimensional stratification parameter	$[mK^{-1}]$
Da	Darcy number	-
Gr	Grashoff number	-
Pr	Prandtl number	-
$\bar{T}$	temperature of the fluid in Laplace domain	$[K]$
$\bar{T}$	dimensionless temperature of the fluid	-
T'	dimensional temperature of the fluid	$[K]$
T_0	temperature of the plate at $y = 0$	$[K]$
T_1	temperature of the plate at $y = 1$	$[K]$
t'	dimensional time	$[s]$
t	dimensionless time	-
U'	dimensional velocity of the fluid	$[ms^{-1}]$
$\bar{U}$	dimensionless fluid velocity in Laplace domain	-
U	dimensionless fluid velocity	-
$\bar{\tau}_1$	transient state skin friction on the plate at $y = 1$	-
$\bar{N}u_1$	transient state rate of heat transfer on the plate at $y = 1$	$[Ws^{-1}]$
$\bar{Q}$	volumetric mass flux rate	$[cm^3 s^{-1}]$

Appendix B

$$A_1 = \frac{1}{p\cosh(\delta)}, \quad A_2 = 0 \quad B_1 = \frac{a}{2DaGr} + \frac{1}{2}\sqrt{\left(\frac{a}{DaGr}\right)^2 - \frac{4\gamma SPr}{Gr}},$$

$$B_2 = \frac{a}{2DaGr} - \frac{1}{2}\sqrt{\left(\frac{a}{DaGr}\right)^2 - \frac{4\gamma SPr}{Gr}}$$

$$D_1 = -\frac{1}{2}\left(\frac{p}{Gr} + \frac{a}{GrDa} - \frac{\gamma pPr}{Gr}\right) + \frac{1}{2}\left(\sqrt{\left(\frac{p}{Gr} + \frac{a}{GrDa} - \frac{\gamma pPr}{Gr}\right)^2 - \frac{4\gamma SPr}{Gr}}\right)$$

$$D_2 = -\frac{1}{2}\left(\frac{p}{Gr} + \frac{a}{GrDa} - \frac{\gamma pPr}{Gr}\right) - \frac{1}{2}\left(\sqrt{\left(\frac{p}{Gr} + \frac{a}{GrDa} - \frac{\gamma pPr}{Gr}\right)^2 - \frac{4\gamma SPr}{Gr}}\right)$$

$\delta_1 = \sqrt{\left(pPr - \frac{D_1 Gr}{\gamma}\right)}$, $\delta_2 = \sqrt{\left(pPr - \frac{D_2 Gr}{\gamma}\right)}$, $\alpha_1 = \sqrt{\frac{B_1 Gr}{\gamma}}$ and $\alpha_2 = \sqrt{\frac{B_2 Gr}{\gamma}}$

References

1. Yuan, Y., Xu, K. and Zhao, K. Numerical analysis of transport in porous media to reduce aerodynamic noise past a circular cylinder by application of porous foam. *Journal of Thermal Analysis and Calorimetry-Springer*. https://doi.org/10.1007/s10973-019-08619-5. 2019.
2. Ismail, A.K., Ibrahim, N.H., Shamsuddin, K.A., Abdullah, M.Z. and Zubair, M. A practical approach in porous medium combustion for domestic application: A review IOP Conference. Series: Material Science and Engineering. https://doi.org/10.1088/1757-899X/370/1/012004. 2018.
3. Vafai, K. Porous media Applications in Biology in systems and Biotechnology, CRC Press ISBN 9780367383671. 2019.
4. Andreas, S.K., Joaquin, J.M. and Denise, M.M. Transport of Nano- and Micro plastic through Unsaturated Porous Media from Sewage Sludge Application. *Environmental Science and Technology*, 2020, **54(2)**, 911-920.
5. Vadi, R. and Sepanloo, K. An improved porous media model for nuclear reactor analysis. *Nuclear Science Technology*, 2016, 27, 24.
6. Eldabe, N.T., Elogail, M.A. and Elshaboury, S.M. Hall effects on the peristaltic transport of Williamson fluid through a porous medium with heat and mass transfer. *Applied Mathematical Modelling*, 2016, **40(1)**, 315-328.
7. Khaled, S.M, Soliman, R.K. and Abduelsalam, S.I. Simultaneous effects of magnetic field and space porosity on compressible Maxwell fluid transport induced by a surface acoustic wave in a micro-channel Chinese Physics B., 22 (12): 124702-1- 124702-10. 2013.
8. Soliman, R.K, El-Sayed, I.B. and Abduelsalam, S.I. Hall and Porous Boundaries Effects on Peristaltic Transport through Porous Medium of a Maxwell Model. *Transport Porous Media*., 2012, **94**, 643-658.
9. Khaled, A.R.A. and Vafai, K. The role of porous media in modeling flow and heat transfer in biological tissues. *International Journal of Heat and Mass Transfer*, 2003, **46**, 4989-5003.
10. Vafai, K. Handbook of porous media, 2nd Ed. Taylor and Francis Group, LLC. 2005.
11. Pop, I. and Ingham, D.B. Convective Heat Transfer: Mathematical and Computational Modeling of Viscous Fluids and Porous media, Pergamon, Oxford. 2001.
12. Gurminder, S., Sharma, P.R. and Chamkha, A.J. Effect of thermally stratified ambient fluid on MHD convective flow along a moving non-isothermal vertical plate, *International Journal of the Physical Science*., 2010, **5(3)**, 208-215.
13. Deka, R.K. and Paul, A. Transient free convection flow past an infinite moving vertical cylinder in a stably stratified fluid. *Journal of Heat Transfer*, 2012, **134**, 1-8.
14. Deka, R.K. and Paul, A. Convectively driven flow past an infinite moving vertical cylinder with thermal and mass stratification. *Pramana Journal of Physics*, 2013, **81(4)**, 641-665.
15. Shapiro, A. and Fedorovich, E. An analytical model of an urban heat island circulation in calm conditions. *Environmental Fluid Mechanics*, 2019, **19**, 111-135.
16. Falasca, S., Moroni, M. and Cenedese, A. Laboratory simulations of an urban heat island in a stratified atmospheric boundary layer, *Journal of Visualization*, 2013, **16(1)**, 39-45.
17. Deka, R.K. and Bhattacharya, A. Magneto-hydrodynamic (MHD) flow past an infinite vertical plate immersed in a stably stratified fluid. *International Journal of the Physical Science*, 2011, **6(24)**, 5831-5836.
18. Vajravelu, K. and Prasad, K.V. Mixed convection heat transfer in an Anisotropic porous medium with oblique principal axes, *Journal of Mechanics*, 2014, **30(4)**, 327-338.
19. Bera, P. and Khalili, A. Double-diffusive natural convection in an anisotropic porous cavity with opposing buoyancy forces: multi-solutions and oscillations. *International Journal of Heat and Mass Transfer*, 2002, **45**, 3205-322.
20. Karmakar, T. and Sekhar, G.P.R. Effect of anisotropic permeability on fluid flow through composite porous channel, *Journal of Engineering Mathematics*., 2016, **100**, 33-51.
21. Yovogan, J. and Degan, G. Effect of anisotropic permeability on convective heat transfer through a porous river bed underlying a fluid layer. *Journal of Engineering Mathematics*, 2013, **81**,127-140.
22. Degan, G., Akowanou, C., Fagbemi, L. and Zinsalo, J. Hydrodynamic Anisotropy Effects on Radiation-Mixed Convection Interaction in a Vertical Porous Channel. *Applied Mathematics*, 2016, **7**, 22-39.
23. Filip, D.A., Pop, I., and Trimbitas, R.T. Fully developed assisting mixed convection through a vertical porous channel with an anisotropy permeability: case of heat flux. Proceedings of the 5th International Conference on Applications of Porous Media, Romania, (International Conference on Applied Physics and Mathematics 2013). Cluj University Press, 2013.
24. Filip, D.A, Trimbitas, R.T and Pop, I. Fully developed mixed convection through a vertical porous channel with an anisotropic permeability: case of heat flux. *Studia Universitis Babes-Bolyai Mathematics*., 2015, **60(2)**, 341-350.
25. Ziyaddin, R. and Huseyin, K. Two-phase steady flow along a horizontal glass pipe in the presence of the magnetic and electrical fields. *International Journal of Heat and Fluid Flow*, 2007, **29**, 263-268.

26. Jha, B.K. and Apere, C.A. Unsteady MHD Couette flows in annuli: The Riemann-Sum approximation Approach. *Journal of the Physical Society of Japan*, 2010, **79**, 1-5.
27. Jha, B.K. and Isa, S. Computational treatment of MHD transient natural convection flow in a vertical channel due to symmetric heating in the presence of induced magnetic field. *Journal of the Physical Society of Japan*, 2013, **82**, 1-9.
28. Tzou, D.Y. Macro to Micro scale heat transfer; the lagging Behaviour. Taylor and Francis, London.1997.
29. Paul, T., Singh, A.K. and Mishra, A.K. Transient natural convection between two vertical walls filled with a porous material having variable porosity. *Mathematical Engineering in Industry*., 2001, **8(3)**, 177-185
30. Jha, B.K. Transient natural convection through vertical porous stratum. *Heat and Mass Transfer*, 1997, **33**, 261-263.
31. Jha, B.K. and Singh, A.K. Transient free-convection in a vertical porous due to symmetric heating. *International Journal of Applied Mechanics and Engineering*, 2003, **8(3)**, 497-502.
32. Liakopoulos A.C. Darcy's coefficient of permeability as symmetric tensor of second rank. *Hydrological Sciences Journal*, 1965, **10(3)**, 41-48.

Received 20 May 2020
Accepted 16 August 2020